AC Conduction Mechanism in Perovskite-like Dimers $(C_2H_8NO)_2M_2X_6$, M=Co/Cu, X=Cl/Br

M. F. Mostafa and S. S. Montasser

Department of Physics, Faculty of Science, Cairo University, Giza, Egypt

Reprint requests to Dr. M. F. M. ⟨mohga@mailer.scu.eun.eg⟩

Z. Naturforsch. **55a,** 945–956 (2000); received October 9, 2000

AC conductivities at 5 Hz–10 kHz and 78 K up to room temperature of bis- (ethanolammonium) Co_2X_6, and bis- (ethanolammonium) Cu_2X_6, X=Cl and Br are reported. At high temperatures, band type conduction prevails for all dimers. In the low temperature range $T<200$ K the $(Co_2Br_6)^{-2}$ dimer conducts via small polarons and the other three dimers conduct via quantum mechanical tunneling. The obtained relaxation times for the different dimers were found to be $1.1 \cdot 10^{-14}$ s. The frequency dependence follows the universal power law $\sigma_{ac}(\omega) = A\omega^s$. The exponent s and the pre-factor A were found to be very sensitive to the phase transitions, with s showing a minimum or maximum at the transition temperature. Changes in the conduction mechanism are reflected by abrupt changes in the variation of the pre-factor A vs $1/T$ relation. The conduction is found to depend on the type of the halide ion rather than on the transition metal ion.

PACS #76, 74.

Key words: AC Conductivity; Phase Transition.

1. Introduction

Materials of perovskite-like structure have for technological reasons been under current investigation [1–3]. To such systems belong the ethanol-ammonium metal halide dimers $(C_2H_8NO)_2M_2X_6$, with M=Co/Cu and X= Cl/Br, for which the dielectric permittivity, structural transformation and magnetic interactions have been studied [4–6]. The room temperature, structural analyses have indicated that the chloride and bromide salts crystallize triclinic ally [6]. The structure consists of nearly planar $(Cu_2Cl_6)^{2-}$ dimers, stacked to form infinite chains. The coordination of the Cu atom is distorted square pyramidal with the ethanol-ammonium oxygen semi-coordinated to the sixth coordination site for each copper atom. The bromide dimers show short-range magnetic interactions at temperatures below <200 K [4, 6] with an ordering temperature of 77 K for the copper bromide dimer. The chloride dimers are paramagnetic above 78 K [4, 6]. Structural phase transformations have been observed in these compounds using differential thermal scanning and dielectric permittivity [4, 5]. The transition temperatures are listed in Table 1. The cobalt bromide dimer undergoes ferroelectric displacive-type transitions at 220 K and an order disorder transition at 302 K. The cobalt chloride dimer shows also two transitions, the first being a displacive ferroelectric one at 210 K with critical slowing down, the second occurs at 282 K and is inactive in the electric permittivity measurements. A similar transition was found in the corresponding copper bromide dimer at 245 K. The other transitions listed in Table 1 are order disorder transitions. It is the aim of this work to study the transport mechanism in these dimers and the role played by the metal ions.

Table 1. Thermodynamic parameters of $(C_2H_8NO)_2Co_2X_6$ and $(C_2H_8NO)_2Cu_2X_6$, X=Cl/Br.

Compound	T^* (K)	ΔH (J/mol)	ΔS (J/mol-deg)
ECOC	195.0	1186.4	5.92
	282.1	568.8	2.01
ECOB	217.29	1395.2	6.4
	301.16	3601.0	11.95

* The temperatures quoted are for onset temperature values.

2. Theoretical Background

Different models have been suggested for the conduction mechanism in glasses and amorphous semiconductors [7, 8], and especially in polycrystalline perovskites [9]. In what follows, two models that are used to analyze the experimental results will be briefly described.

2.1. Quantum Mechanical Tunneling (QMT)

The conductivity due to a single electron motion undergoing QMT is given by [8, 10]

$$\sigma = (\pi^4 e^2 kT/384)\,[N(E_F)]^2\,\alpha^{-5}\omega \ln^4(1/\omega\tau_0), \quad (1)$$

0932-0784 / 2000 / 1100-0945 $ 06.00

where τ_0 is the characteristic relaxation time (of the order of the inverse phonon frequency). The other parameters are defined in [10]. The hopping distance at a particular frequency is given by

$$R_\omega = (2\alpha)^{-1} \ln (1/\omega \tau_0). \quad (2)$$

The frequency exponent s in this model is given by

$$s = 1 - 4/\ln (1/\omega \tau_0). \quad (3)$$

For the QMT model the ac conductivity is linearly dependent on the temperature, and the frequency exponent is temperature independent.

A temperature dependent frequency exponent can be obtained within the framework of the QMT model in the pair approximation by assuming that the carriers form non-overlapping small polarons (SP). In this case, the frequency exponent becomes [10]

$$s = 1 - 4/[\ln (1/\omega \tau_0) - W_H/kT]. \quad (4)$$

This expression results in a temperature dependent s that increases with increasing temperature [10]. The tunneling distance in the non-overlapping small polaron becomes

$$R_\omega = (2\alpha)^{-1} [\ln (1/\omega \tau_0) - W_H/kT], \quad (5)$$

where the minimum value of R_ω corresponds to the interatomic spacing.

2.2. Correlated Barrier Hopping (CBH)

A model for ac conduction which correlates the relaxation variable W with the intersite separation R was originally developed by Pike [11] for single electron hopping and extended by Elliott [10] for simultaneous two-electron hopping. For neighboring sites at a separation R, the Coulomb wells overlap, resulting in lowering of the effective barrier height from W_m to W, which for two – electron hopping is given by

$$W = W_m - 2e/\pi \varepsilon \varepsilon_0 R_\omega, \quad (6)$$

where ε is the dielectric constant of the material and ε_0 that of the free space. The ac conductivity for CBH in the narrow band limit is given by

$$\sigma(\omega) = (\pi^3/12) [N (E_F)]^2 \varepsilon \varepsilon_0 \omega R_\omega^6, \quad (7)$$

where N is the concentration of site-pairs, the hopping distance R_ω is given by

$$R_\omega = 2 e^2/\pi \varepsilon \varepsilon_0 [W_m - kT \ln (1/\omega \tau_0)] \quad (8)$$

and the frequency exponent s by

$$s = 1 - 6 kT/[W_m - kT \ln (1/\omega \tau_0)]. \quad (9)$$

In this model, a temperature dependent frequency exponent is predicted with s increasing towards unity as the temperature decreases.

3. Experimental Details

3.1. Samples

Sample preparation and identification are described in [4, 5].

3.2. AC Conductivity Measurements

The conductivity measurements in the frequency range 5 Hz–10 kHz, were carried out using a computer controlled lock-in amplifier type PAR 5207. The temperature was measured with a copper constantan thermocouple. The powdered samples were pressed under two tons/cm^2 to pellets of 8 mm diameter and 1.0 mm thickness. The plane surfaces were coated with silver paste. The samples were first cooled to liquid nitrogen temperature. Then the measurements were carried out while heating the sample. The measuring technique and precautions to avoid stray capacitance are discussed in [12].

4. Results

4.1. Temperature Dependence

4.1.1. (Bis-ethanol-ammonium) hexa-chloro-cobaltate (ECOC)

The variation of the ac conductivity as a function of temperature at selected frequencies for the ECOC dimer is shown in Figure 1 (a). Four regions may be identified, which are denoted by regions, (I), (II), (III), and (IV). In region (I), a frequency dependent and nearly temperature independent conductivity is observed. This is associated with a very small, frequency independent activation energy ($\Delta E \sim 21$ meV), reflecting an extrinsic type of conduction. At higher temperatures, region (II), the conductivity is frequency- and temperature-dependent, with a large, frequency dependent activation energy. The variation of the activation energy observed in this region is plotted in the insert 1 (c). The frequency dependence of the activation energy is fitted to the equation [13].

$$\Delta E = \Delta E_0 [1 - \exp (-f_0/f)]^\gamma, \quad (10)$$

where ΔE_0 is the activation energy at $f = 0$ and γ is constant. Values of ΔE_0, f_0, and γ are listed in Table 2. In

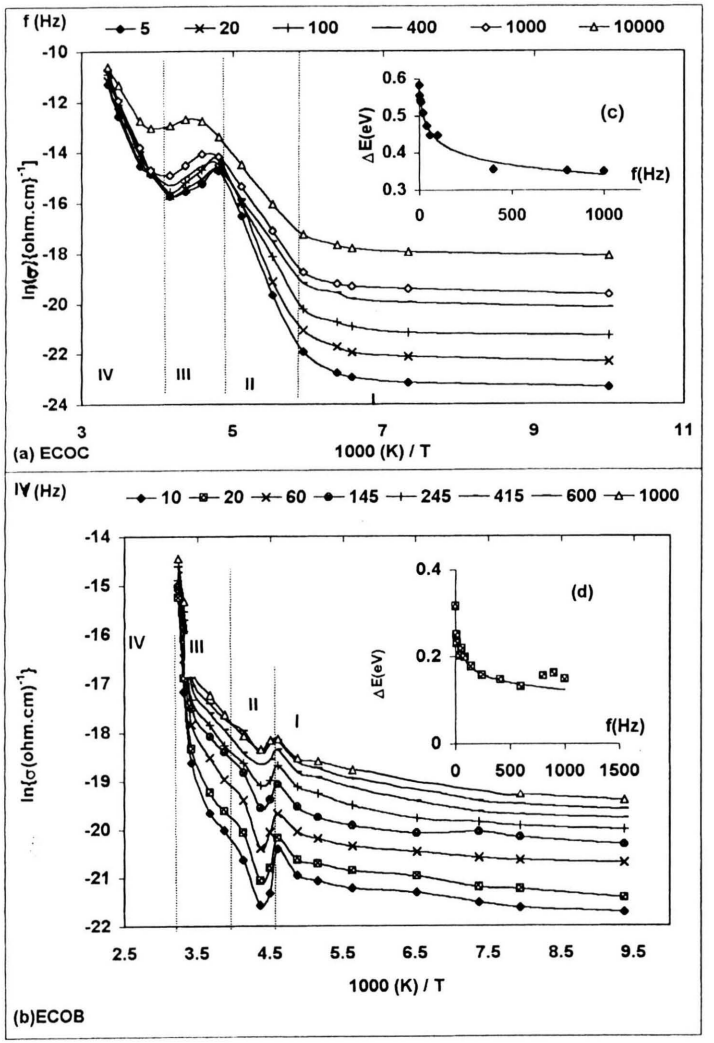

Fig. 1. The variation of the ac conductivity as function of 1000/T for ECOC (a) and for ECOB (b) at selected frequencies. (c) Variation of the activation energy as function of frequency (f), dots are experimental results and lines are fit to [11] for ECOC and for ECOB (Fig. 1d).

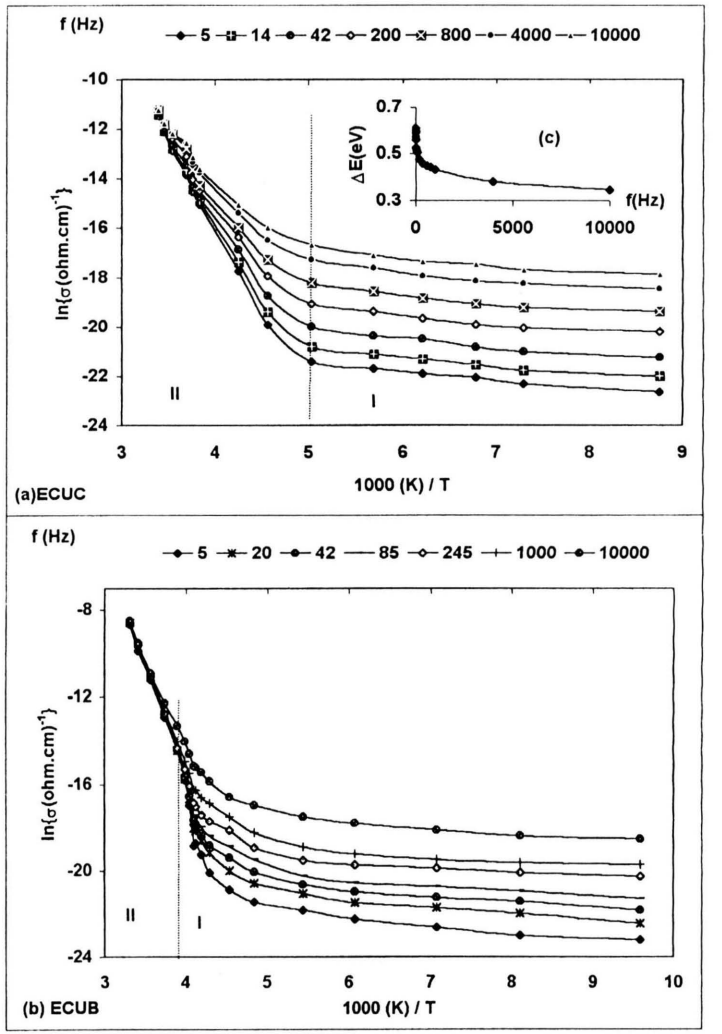

Fig. 2. (a) The variation of the ac conductivity as function of 1000/T for ECUC (a) and for ECUB (b) at selected frequencies. (c) Variation of the activation energy as function of frequency (f), dots are experimental results and lines are fit to [11] for ECUC.

Table 2. Values of ΔE_0, f_0, and γ as obtained from the fitting of [11].

Dimer	ΔE_0 (eV)	f_0 (Hz)	γ
ECOC	0.6	7.9	0.11
ECOB	0.25	26.7	0.19
ECUC	0.95	19.9	0.15

region (III), which corresponds to the ferroelectric phase [4], the activation energy is negative. In region (IV) the frequency independent conductivity, with an activation energy of $\Delta E = (0.62 \pm 0.02)$ eV, is in the range of ionic conduction.

4.1.2. (Bis-ethanol-ammonium) hexa-bromo-cobaltate (ECOB)

The variation of the ac conductivity as function of temperature at selected frequencies for the ECOB dimer is shown in Figure 1(b). Four regions are found, which are denoted by regions (I), (II), (III), and (V). In region (I), the conductivity is non-Arrhenius and frequency dependent. In region (II) ($217\ \text{K} < T < 240\ \text{K}$), which corresponds to the ferroelectric regime [4], the conductivity decreases with increasing temperature; this decrease is a function of the frequeny, being larger at lower frequencies. The decrease in conductivity with increasing temperature reveals a negative activation energy. Region (III) is characterized by Arrhenius type behavior with the conductivity being frequency dependent. The variation of the activation energy observed in this region is plotted in the insert 1 (d). This was fitted to (10). The values of ΔE_0, f_0, and γ are listed in Table 2. A sudden rise in the conductivity at $T \sim 300$ K (marking the beginning of region (IV)) is observed where dc conduction prevails, with a large activation energy $\Delta E \cong 1.18$ eV. The frequency independent activation energy is in the range of ionic conduction.

4.1.3. (Bis-ethanol-ammonium) hexa-chloro-cuprate (ECUC)

The variation of the ac conductivity as function of temperature at selected frequencies for the ECUC dimer is shown in Figure 2(a). It is noted that at higher temperatures, region (II), the conductivity is high and that it decreases as the temperature decreases, following Arrhenius' law, but a marked difference in found in this variation depending on the frequency and temperature ranges. At low frequencies ($f = 5$ Hz) and high temperatures, σ_{ac} decreases faster than at high frequencies ($f =$ 10 kHz), while below 200 K (region I) the decrease is frequency independent and reduces slightly with further decrease in temperature. This is reflected in different activation energies at different frequencies for $T > 200$ K but with the same activation energies for $T < 200$ K. The variation of the activation energy with frequency at $T > 200$ K is seen in the insert (c). It can also be seen that at low temperatures, region (I), the conductivity shows weak dependence on temperature and strong dependence on frequency. This is typical for an extrinsic type of conduction.

4.1.4. (Bis-ethanol-ammonium) hexa-bromo-cuprate (ECUB)

The variation of the ac conductivity as function of temperature at selected frequencies for the ECUB dimer is shown in Figure 2(b). It is clear that at lower temperatures, region (I), the ac conductivity shows a weak dependence on temperature and strong dependence on frequency, while at higher temperatures, region (II), the conductivity is frequency independent, showing strong dependence on temperature following Arrhenius' law. The values of the activation energy of $\Delta E \sim 1.0$ eV reveals ionic type conduction.

4.2. Frequency Dependence

4.2.1. Bis-ethanolammonium hexa-chloro-cobaltate (ECOC)

Figure 3 shows the frequency dependence of ln $(\sigma_T(\omega))$ as function of ln (ω) for the ECOC dimer at different temperatures as a representative example for all dimers. It can be seen from this Figure that at lower temperatures ac conductivity dominates. As the temperature increases, the temperature at which the dc conductivity predominates, varies from one dimer to another, and is found to be 240, 290, 260, and 240 K for ECOC, ECOB, ECUC, and ECUB, respectively.

4.3. Dielectric Modulus

In the high temperature region there are no well defined relaxation peaks in the dielectric loss, thus we are going to use the dielectric modulus formalism [14] to analyze the high temperature data for the four compounds.

Figure 4(a) and 4(b) show the real (M') and the imaginary (M'') parts of the dielectric modulus ($M^* = 1/\varepsilon^*$) as function of ln (ω) for ECUB dimers, which is typical for all four dimers. An S shaped M'–ln (ω) relation and a

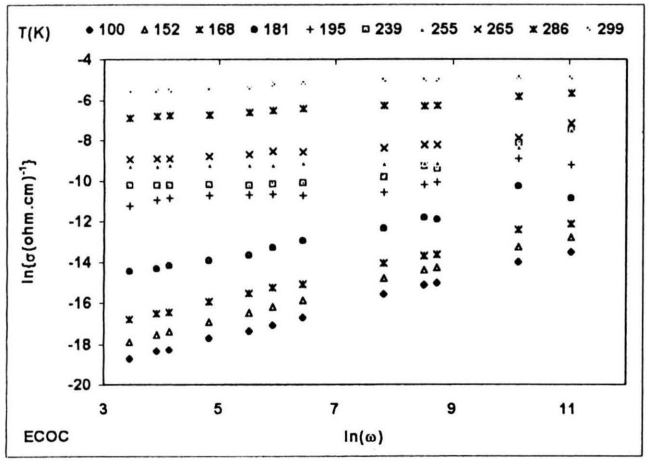

Fig. 3. The variation of the ac conductivity ln (σ_T) as function frequencies ln (ω) for ECOC as a representative for all other dimers.

Table 3. Values of the β, ε_∞, and activation energy for the relaxation process at different temperatures.

Compound	$T(K)$	β	ε_∞	ΔE (eV)
ECOC	195–207	0.15–0.18	14.7–16.1	
	217–255	0.1 –0.12		
	265–298.9	0.22–0.26	16.7–208	0.047
ECOB	228–257	0.07–0.13	11.1–11	
	272–308	0.35–0.27	11.2–12.5	0.026
ECUC	272–300	0.25–0.17	71–83	0.23±0.05
ECUB	242–267	0.69–0.28	6.67–9.9	0.25±0.02
		(0.16–0.05)	125–200	
	272–308	0.0	400	

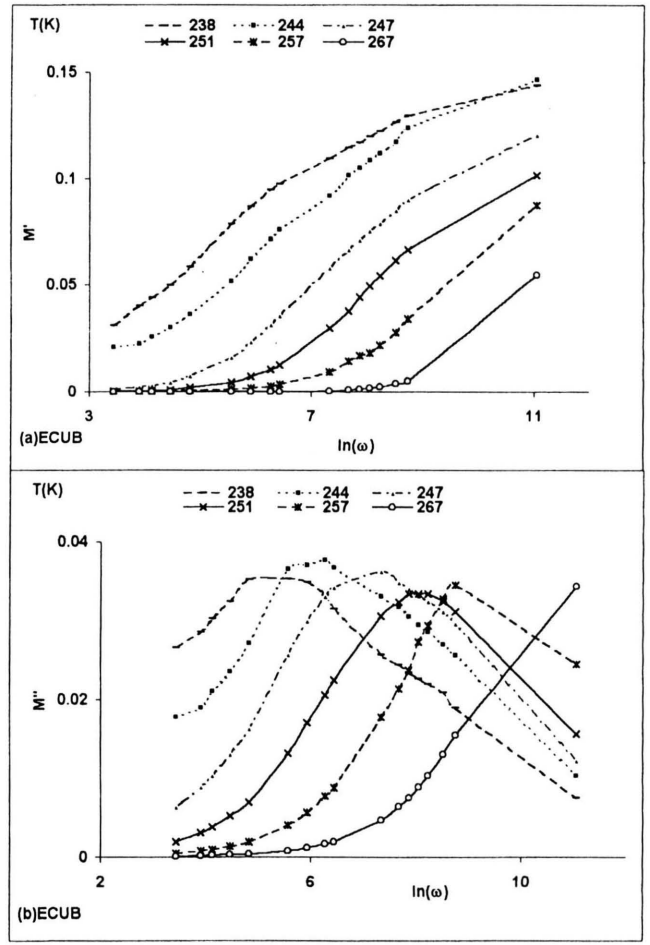

Fig. 4. Variation of the dielectric modulus (M^*)-ln ω for ECUB as a representative for all dimers.

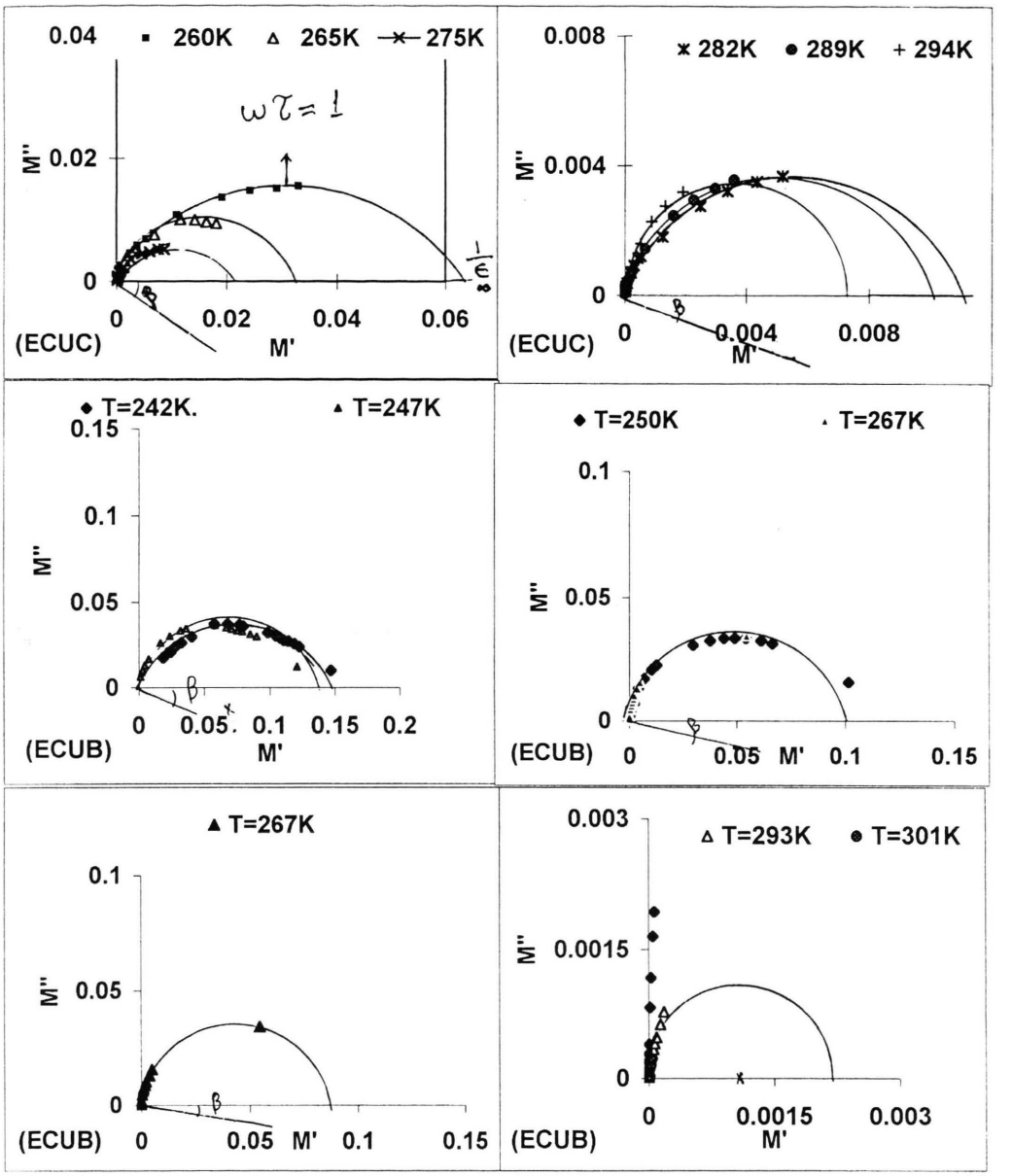

Fig. 5a. Dielectric modulus M'' vs. M' at selected temperatures for ECUC and ECUB.

peak in the M''–ln (ω) relation which is typical ionic conduction [14]. This agrees with our conclusion of ionic conduction at high temperatures obtained from the activation energy values. Figure 5(a) shows the relation of M'–M'' for ECUC and ECUB as representative examples for the chloride and bromide dimers, respectively. Similar results were obtained for the cobalt dimers, where semi-circular arcs are obtained [4, 15]. The values of ε_∞ and α, as obtained from these plots are listed in Table 3. The relation between the relaxation times as obtained from $\omega\tau = 1$, plotted as function of the reciprocal temperature are shown in Figure 5 (b). The values of the activation energies for the relaxation process of all dimers are listed in Table 3.

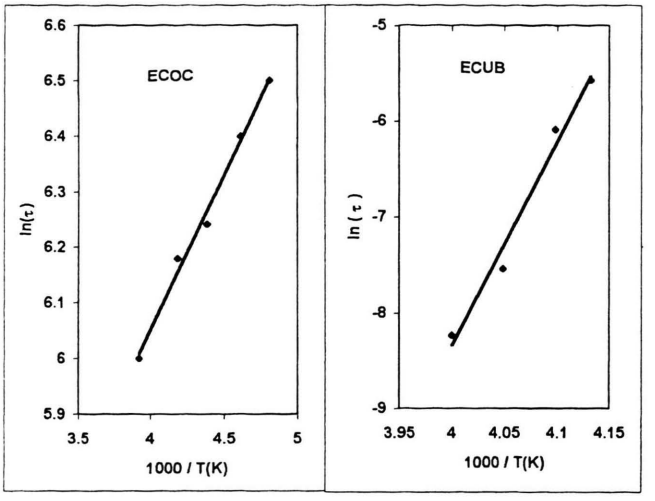

Fig. 5b. Relaxation time (τ) vs $1000/T$ (K) for ECUC and ECUB.

Table 4. Activation energies at different regions for the $[C_2H_8ONO)_2\ Co_2X_6$ and $[C_2H_8ONO)_2\ Cu_2X_6$, X=Cl/Br at different temperature regions.

Compound	T (K)	ΔE (eV)	ΔE (eV) from ln (A)
ECOC	(I) $T<170$	0.021 ± 0.005	0.025
	(II) $170<T<250$	0.56 (10 Hz)	0.54
		-0.24 (10 kHz), 0.58 at $f=0$	
	(IV) $T>210$	0.62 ± 0.02	
ECOB	(I) $T<200$	No-Arrhenius	0.0017
	(III) $220<T<300$	0.21 ± 0.02	0.38
	(IV) $T>300$	1.18 ± 0.11	
ECUC	(I) $T<200$	0.021 ± 0.005	0.029
	(II) $T>200$	0.62 ($f=5$ Hz)	0.69
ECUB	(I) $T<245$	0.038 ± 0.04	0.038
	(I′) $220<T<250$		0.61
	(II) $T>250$	1.010 ± 0.007	

5. Discussion

As seen from Fig. 3, the conductivity follows the universal power law

$$\sigma_{ac}(\omega) = A\,\omega^{s(T)}, \tag{11}$$

where A is a temperature – dependent constant and s is the universal exponent which usually has values between 0 and 1.

In order to obtain accurate fits for the conductivity-(ω) relation, one has to subtract values of σ_{dc} from the total measured ac conductivity, especially in temperature regions where both are equally dominant. This was carried out by extrapolating the values of $\sigma_T(\omega)$ to get $\sigma(0)$ at every temperature for the four dimers, and then we used the universal power law to get the values of $A(T)$ and $s(T)$ through least squares fitting of [11].

5.1. Low Temperature Range

5.1.1. Variation of $s(T)$ and $A(T)$

In the temperature range $T \leq 200$ K, the ac conductivity is substantially higher than the dc conductivity and is found to follow the universal power law as given by [11]. The temperature at which the dc contribution becomes significant varies somewhat from one material to another. Calculations of the universal exponent s and the prefactor A were carried out in regions where the ac contribution predominates.

Figure 6 depict the variations of s and ln (A) as function of T and $1/T$ respectively. Three regions are identified in Figs. 6 (a) and 6 (b). Region (I) shows an almost temperature independent s which corresponds to a thermally activated A, with an activation energy 0.028 eV. This activation energy is very close to that obtained from the Arrhenius plot of Fig. 1 (a) in the same temperature regime. In region (II), s is found to decrease with increasing T, reaching a minimum at (210 ± 2) K. In this region, Fig. 6 (b) shows ln (A) to increase gradually, reaching a maximum at the same temperature (210 ± 2) K. The rate of increase of ln (A) with $1/T$ reflects a thermally activated behavior with an activation energy 0.54 eV. This value is in very good agreement with that obtained from the Arrhenius plot of Fig. 1 (a) (region II). It is to be pointed out that the observed minimum at (210 ± 2) K found in the $s-T$ relation corresponds to the maximum in the ln (A) vs. $1/T$ relation, which is the temperature where ferroelectric transition occurs, as was previously observed [4]. Figures 6 (c) and (d) show different behavior, where s shows a maximum at the ferroelectric transition while ln (A) shows a minimum at the temperature, (217 ± 4) K. Yet, it is to be noted that a thermally activated behavior with very small activation energy was obtained for region (I), and an activation energy of 0.26 eV in region (II), which is about the same as that obtained from Fig. 1 (b) in the same temperature regime. The minimum and maximum peaks, indicated by arrows, correspond to transition temperatures obtained from DSC measurements as listed in Table 1, and were found to correspond to a ferroelectric transition [4]. It is interesting to note that, while s may indicate a maximum, ln (A) will be a minimum and vice versa, these minima or

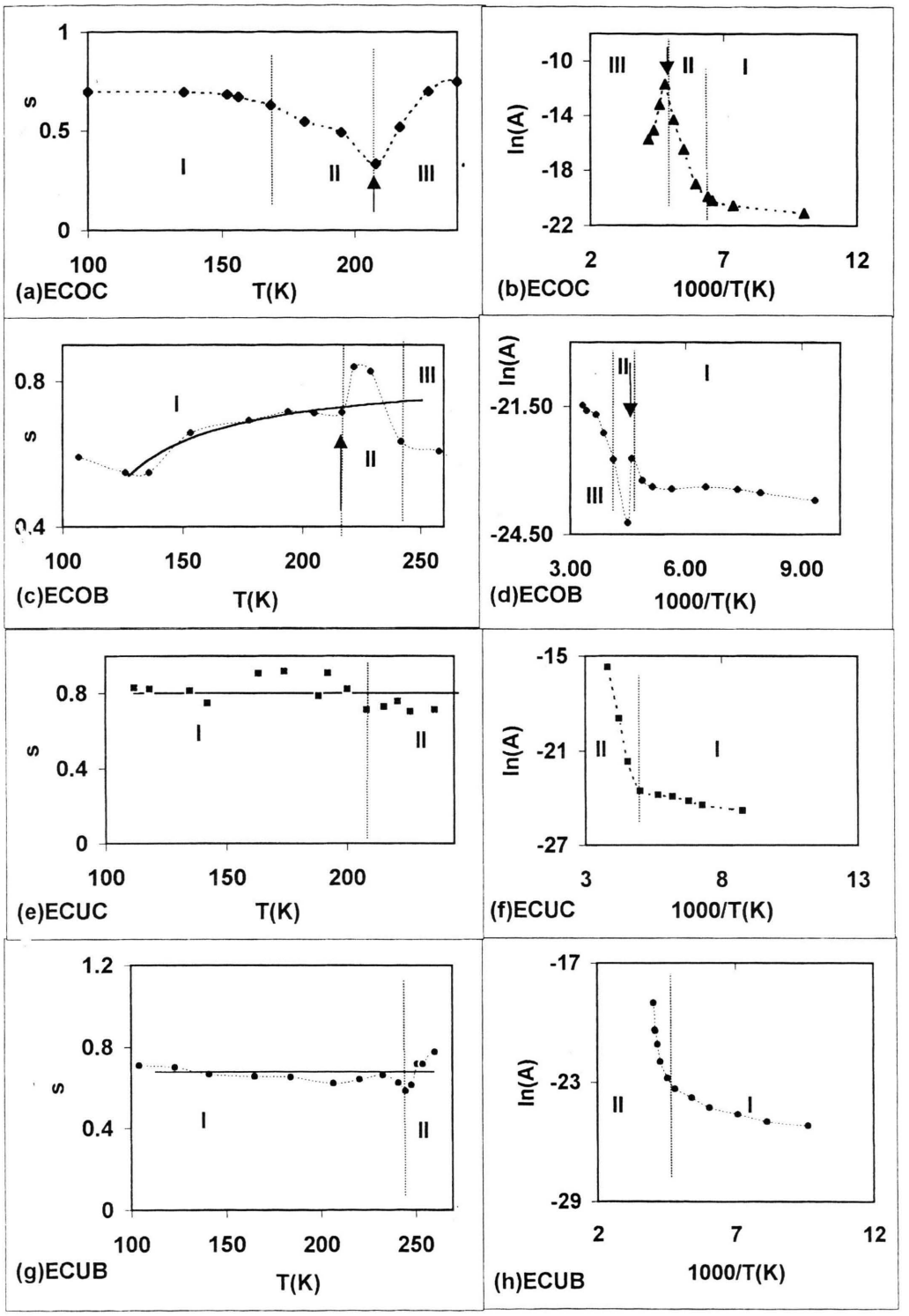

Fig. 6(a–h). Variation of the universal exponent (s) and the pre-factor ln (A) as function of temperature for ECOC, ECOB, ECUC, and ECUB.

maxima being very sensitive to structural or electrical phase transformations. As was previously found, the ECOC and ECOB dimers undergo displacive phase transitions at (210 ± 2) K and (271 ± 4) K, however the nature of the transitions is different [4]. This is reflected in their s- and ln (A) variation with temperature.

In the case of ECUC and ECUB, neither minima nor maxima were observed in the variation of s or ln (A) with T [Fig. 6 (e), (f), (g) and (h)] instead, a change in the slope is noted at 200 and 240 K, respectively. This can be attributed to a change in the conduction mechanism, where ac conduction prevails on the low temperature side, region (I), and the dc conductivity is dominant in region (II). The activation energies obtained in the different regions are listed in Table 4, and are found to agree with those obtained from Arrhenius relations. Similar results were obtained for Mn-perovskites [9]. We can thus suggest that abrupt changes in the electric and/or structural properties of a material can be associated with a minimum or maximum in the $s-T$ relation, which in turn is associated with a maximum or minimum in the ln (A) – T relation. Changes in the conduction mechanism are reflected as variations in the s and/or ln (A) dependence on T.

5.1.2. AC conduction mechanisms

As pointed out in Sect. 2 several models based on quantum mechanical tunneling (QMT) and classical hopping of charge carriers have been proposed to account for the dependence of the ac conductivity on frequency and its exponent [10]. The model based on QMT of electrons through a barrier predicts a temperature independent s. An increase of s with increasing temperature is found for the case of non-overlapping small polaron tunneling [10]. One the other hand, the model based on classical hopping of electrons over a barrier predicts a decrease of s with increasing temperature [10]. For ECOC, in the temperature range 100 – 170 K, where s is temperature independent, we fitted the data to the QMT model. A reasonable fit for $\sigma_{ac} - \omega$ at different temperatures was obtained, as seen in Figure 7 (a). Yet, when applying the QMT model to the whole temperature range, i.e. up to 200 K, the obtained relaxation time was found to be $\sim 9.28 \times 10^{-9}$ s, which is much higher than would be expected for phonon assisted tunneling. Thus, we have tried to use the CBH over the temperature ranges 100-up to the transition temperature. A critical test for the CBH model comes from the temperature dependence of σ_{ac} and s. Fits of the experimental data (σ_{ac}) as function of frequency using N (E) and τ_0 as variable parameters did not result in good fits over the temperature regions. Hence it is reasonable to assume that the QMT model accounts for the conduction mechanism in the temperature range (I) only, and that a change in the conduction mechanism occurs above that temperature. This agrees with the variation of s and ln A with T. It was not possible to fit the data in the temperature range (II) to a specific model, due to the limited number of data points. Hence we can only say that a change in the conduction mechanism is observed near 170 K, and that in region (I) QMT prevails while ionic hopping takes place in region (II). The suggestion that ionic conduction prevails at $T > 170$ K is supported by the results of the modulus spectroscopy given above.

Table 5. Type of model, relaxation time (τ_0), hopping distance (R), density of states (N (F)), α, and activation energy (W_H).

Dimer	Model	τ_0 (S)	R (A)	N (F)/cc	α	W_H (eV)
ECOC	QMT	9.28×10^{-9}	63	37×10^{22}	0.1	–
	CBH	1.4×10^{-14}	55		–	0.56
ECOB	SP	1.59×10^{-14}	54	9×10^{22}	0.1	0.16
ECUC	QMT	1.44×10^{-14}	121	12×10^{22}	0.1	–
ECUB	QMT	7.5×10^{-9}	62	40×10^{22}	0.1	–

In case of the ECOB, the behavior of s, region (I), is entirely different. A fit of s to QMT is not possible as s is temperature dependent. However, a fit to QMT, with a non-overlapping small polaron, yields very good results and is presented by the solid line of Figure 6 (c). The fit of $\sigma_{ac} - \omega$ at different temperatures to the non-overlapping small polaron model is plotted in Fig. 7 (b), which is found to be quite reasonable. The relaxation times τ_0 and W_H obtained from the fit are listed in Table 5. We did not try to fit the intermediate temperature region where the transition occurs. Conduction in region (II) is attributed to ionic type as found from the modulus plots.

It is to be noted that, although these two compounds are isomorphous at room temperature, they behave differently at low temperatures. This can most likely be attributed to the fact that they undergo phase transitions of different mechanisms. As reported earlier [4], this difference is related to the fact the ECOB shows magnetic interactions at low temperatures, while ECOC does not. Thus, we can relate the difference in their conduction mechanism to the difference in their magnetic behavior.

In the case of copper dimers, the s value obtained for ECUC, [as seen in Fig. 6 (e)] in the temperature range

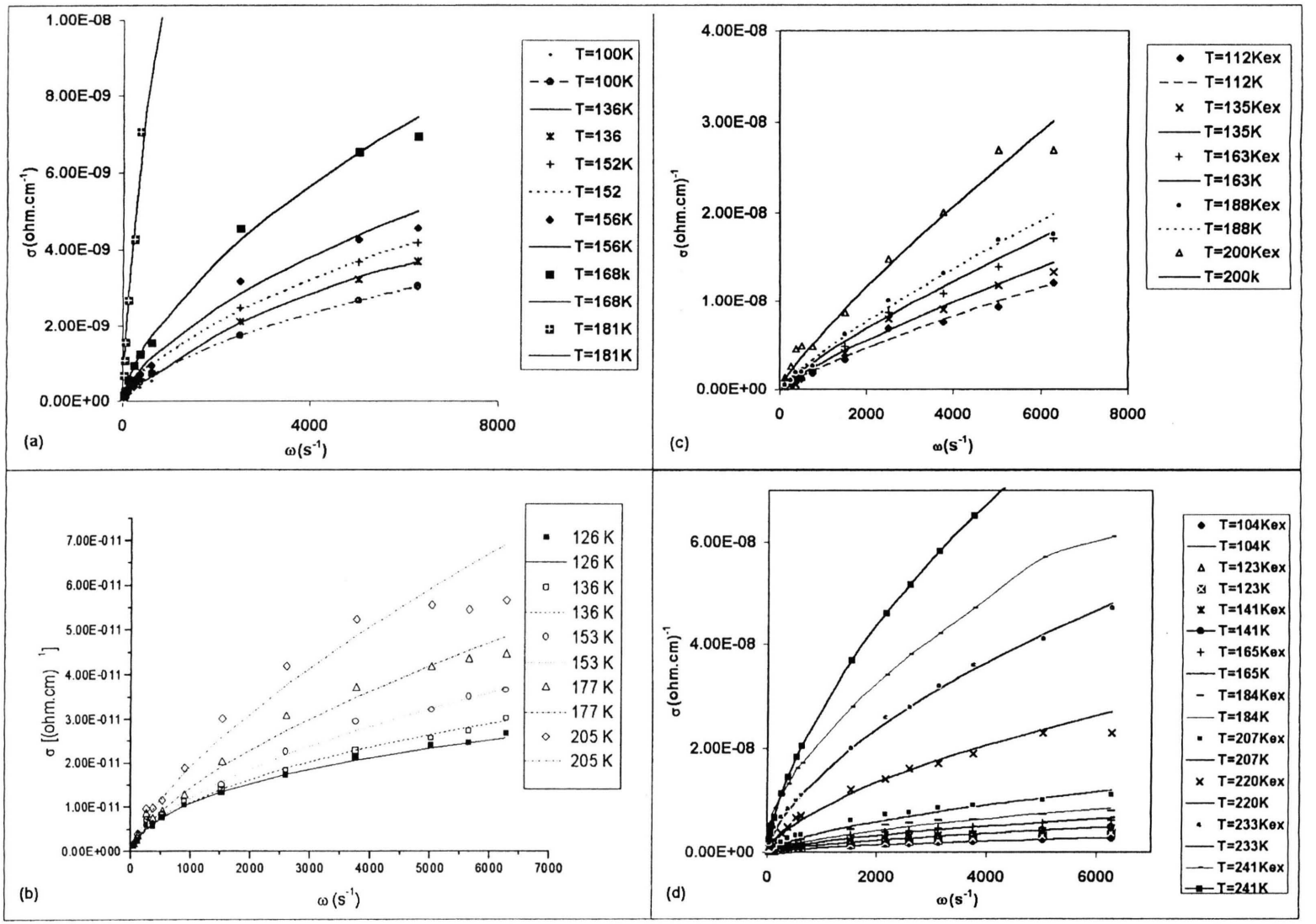

Fig. 7 (a–d). The ac conductivity fit to the different models for the four dimers. The dots are the experimental points and the lines are the results of the fit.

(I), is temperature independent ($T < 200$ K) and has a value of nearly 0.8, which indicates QMT conduction mechanism. The values of the fitting parameters are listed in Table 5, and the fit of the experimental ac conductivity to this model is shown in Figure 7 (c). The value of the relaxation time (τ_0) of 1.44×10^{-14} s is quite reasonable for phonon-assisted conduction. In the temperature range (II), we suggest ionic type conduction, which is supported by the modulus spectroscopy results.

For ECUB dimer in the temperature range ≤ 230 K, region (I), a temperature independent s [as seen in Fig. 6 (g)], suggests QMT, however, the value of $s \sim 0.67$ yields a value of $\tau_0 \sim 10^{-9}$ s, which is rather large for phonon assisted conduction. This may be related to the fact that in this temperature range ECUB shows short range magnetic interactions, which could very well affect the obtained values of the relaxation time. Values of the fitting parameters are listed in Table 5, and the fit of the experimental ac conductivity to this model is shown in Figure 7 (d). From this figure it can be seen that the fit is quite good. In the temperature range (II), ionic conduction prevails.

5.2. High Temperature Range

Regarding the high temperature results, it is clearly seen:

1. σ_{dc} prevails for all dimers.
2. The activation energies obtained for the chloride dimers (ECOC and ECUC) are equal, $\Delta E \sim 0.6$ eV.
3. The activation energies for the bromide dimers are equal, $\Delta E \sim 1.0$ eV.

One can see from the above remarks that the halide ion plays the major role in the conduction of these dimers. Br, being heavier, would require larger energy values.

It is to be noted that the conductivity of the two chloride dimers in the low temperature region is higher than that of the corresponding bromides. However, at high temperatures, where σ_{dc} predominates, the conductivity for all dimers has within experimental error the same value. This indicates that the conduction mechanism at high temperatures is of different from that at low temperatures.

6. Conclusion

At high temperature, all dimers conduct via the same mechanism. The activation energy depends on the type of halide ion, where the bromide dimers have equal activation energies which are about twice those of the corresponding chlorides. This is an indication that conduction at high temperatures in mainly due to the halide ions and that the transition metal ion does not play a major role in the conduction mechanism.

In the low temperature region, pre-transition, the conduction mechanism for the copper halide dimers, and for the ECOC were found to occur mainly via QMT tunneling. The better fit to small polaron tunneling that was obtained in the case of ECOB is likely to be a result of the presence of magnetic interaction in this temperature range. Needless to say that the transition metal ion does not play a major role in the conduction mechanism at high and low temperatures. This is not surprising since the Cu^{+2} ($3\,d^9$) and Co^{+2} ($3\,d^7$) ions have the same ionic radii and the 3d-electrons of the transition metal ions are irrelevant for the conduction mechanism at $T > 78$ K.

Since the chloride dimers have higher conductivities than the bromides at low temperatures, one may conclude that it is the type of the dimeric unit, $(M_2 X_6)^{-2}$, that affects the conduction. In other words the role played by the transition metal ion is not effective, rather it is the halide ion. This would be expected in light of the difference in the size and the electronegativity of the halide ions. These factors contribute to the difference in the strength and the electronegativity of the halide ions. These factors contribute to the difference in the strength of the N–H…Cl bonding, which is different from that of the N–H…Br bounding, thus affecting the conduction mechanism.

It should be stressed that the theoretical models that were used for the analysis of the results can be considered as a rough guide to understand conduction in these perovskites. They cannot be used to clearly discriminate one mechanism against the other. Most probably, all of the above-mentioned transport channels contribute to the complex conduction mechanism in these strongly polar materials.

[1] L. J. DeJongh and A. R. Miedema, Adv. Phys. **23,** 1 (1974).
[2] M. F. Mostafa and A. S. Atallah, Phys. Lett. **264A,** 242 (1999).
[3] R. Jakubas, G. Bator, P. Ciapala, J. Zalenski, J. Baran, and J. Lefebvre, Cond. Matt. Phys. **7,** 5335 (1995),
[4] M. F. Mostafa and S. S. Arafat, Z. Naturforsch. **6/7a,** 595 (2000).
[5] M. F. Mostafa, S. S. Arafat, and M. M. Abdel-Kader, Phil. Mag. **75B,** 167 (1997).
[6] B. Scott and R. D. Willett, Inorg. Chem. Acta **141,** 139 (1988).
[7] Joncher, Dielectric Relaxation in Solids, Chelsea, Dielectric Press, London 1983.
[8] A. R. Long, Adv. Phys. **31,** 553 (1982).
[9] M. F. Mostafa and A. S. Atallah, l.c. [2].
[10] S. R. Elliott, Adv. Phys. **36,** 135 (1987).
[11] G. E. Pike, Phys, Rev. **B6,** 1572 (1972).
[12] M. F. Mostafa, M. El-Nimer, and F. Reicha, Physica. Scripta **43,** 451 (1993).
[13] M. A. Soliman, F. Reicha, and A. M. Shaban, Polymer Bulletin **27,** 311 (1991).
[14] P. B. Macedo, C. T. Moynihan, and R. Bose, Phys. Chem. Glasses **13,** 171 (1972).
[15] S. S. Arafat, Ph.D. Thesis, Faculty of Science, University of Cairo 1996.